Acta Cryst. (1972). A28, 572

Thermal Diffuse Scattering in Cubic Powder Patterns

BY C. B. WALKER AND D. R. CHIPMAN

Army Materials and Mechanics Research Center, Watertown, Massachusetts 02172, *U.S.A.*

(*Received* 24 *April* 1972 *and in revised form* 1 *June* 1972)

The one-phonon thermal diffuse scattering in powder patterns of monatomic cubic materials has been investigated using a model that gives the correct frequencies and polarization vectors of the long-wavelength phonons for materials of arbitrary elastic anisotropy. Computer calculations have been made of the intensity distribution of this scattering and of the correction for its inclusion in measured integrated intensities of powder pattern reflections. Elastic anisotropy is found to produce marked differences, despite the powder pattern averaging; and, contrary to the Chipman–Paskin approximation, the integrated intensity correction is found generally not to vary smoothly with $(h^2+k^2+l^2)$ or linearly with scan length even for isotropic materials, as Suortti also noted. A much simpler method for calculating the integrated intensity correction has also been developed, based on a modified Warren model, that gives reasonably accurate values under most conditions even for very anisotropic materials and is several orders of magnitude faster than the primary method.

Introduction

Thermal diffuse scattering (TDS) in powder patterns forms a nonuniform background that peaks sharply at the positions of the crystalline reflections and thus is partially included in measurements of integrated intensities of the reflections. The distribution of this scattering in cubic powder patterns has been studied for relatively simple models of the thermal vibrations by Warren (1953), Herbstein & Averbach (1955), Paskin (1958, 1959), Chipman & Paskin (1959*a*), Borie (1961), and Suortti (1967), and the correction for the included TDS in measured integrated intensities from cubic powder patterns has been investigated by Chipman & Paskin (1959*b*), Schoening (1969), and Suortti (1967). Suortti's work is the most sophisticated of these studies, but his isotropic model for the thermal vibrations is still rather simple–all phonons are either pure longitudinal or (doubly degenerate) pure transverse, with the frequencies in each branch being independent of the orientation of the phonon wave vector, **g**; the actual Brillouin zone is replaced by a sphere of equal volume; and the dispersion in each branch is that of a linear chain with the mean long-wavelength velocity of that branch.

The present study employs a more complex model with the advantage that it gives the correct frequencies and polarization vectors of the long-wavelength phonons for cubic materials of arbitrary elastic anisotropy; the actual Brillouin zone is again replaced by a sphere of equal volume, dispersion for each branch in any direction is that for a linear chain with the appropriate long-wavelength velocity, and phonon polarizations are assumed to be independent of the length of the wave-vector. The study has been restricted to one-phonon scattering and to monatomic cubic materials. In the first part of the paper we consider the TDS intensity distribution predicted by our model and show that elastic anisotropy can produce quite marked differences. In the second part we investigate the correction for the included TDS in measured integrated intensities, including numerical calculations to illustrate how it depends on various factors, and compare these results with those from previous approximations. We also develop an alternate, much simpler method for calculating the included TDS correction that is orders of magnitude faster than our primary method and is still reasonably accurate under most conditions even for very anisotropic materials.

Intensity distribution

We consider first the scattering from a single crystal of the monatomic cubic specimen. We assume that the temperature is high enough for there to be equipartition of energy among the phonons. The intensity in electron units of the one-phonon TDS at a point, $\mathbf{H}=\boldsymbol{\tau}+\mathbf{g}$, in reciprocal space, where $\boldsymbol{\tau}$ is the vector to the nearest reciprocal lattice point, can then be written

$$J(\mathbf{H})=\frac{Nf^2\exp(-2M)}{m}k_BT\sum_{gj}\frac{(\mathbf{H}\cdot\mathbf{e}_{gj})^2}{v_{gj}^2}. \qquad (1)$$

N is the number of atoms in the sample; m is the atomic mass; f is the atomic scattering factor; $\exp(-2M)$ is the Debye–Waller temperature factor; k_B is the Boltzmann constant; T is the absolute temperature; and v_{gj} and $\mathbf{e}_{gj}$ are respectively the frequency and the polarization vector for the phonon with wave vector **g** in the jth branch ($j=1,2,3$). This expression is exact for X-ray scattering, but the corresponding relation for neutron scattering is only approximate (Cochran, 1963; Willis, 1969). Note that our wave vectors and other reciprocal

space quantities do not include the factor 2π that is incorporated there in some systems of notation.

The spherical Brillouin zone of our model has a radius, g_m/a, defined by

$$(4\pi/3)\,(g_m/a)^3 = n/v$$

where a is the real cubic lattice parameter; $v(=a^3)$ is the volume of the real cubic unit cell; n is the number of atoms in the cubic unit cell; and g_m is dimensionless for convenience. The assumption of linear chain dispersion for our model gives

$$\begin{aligned} v_{gj} &= V_{gj}|\mathbf{g}|\,\frac{\sin\frac{\pi}{2}\frac{g}{g_m}}{\frac{\pi}{2}\frac{g}{g_m}} \\ &= V_{gj}|\mathbf{g}|\,S(g), \end{aligned} \tag{2}$$

where V_{gj} is the long-wavelength velocity for phonons in the jth branch with wave-vector parallel to $\mathbf{g}$; and $g=a|\mathbf{g}|$, dimensionless. Then, assuming that the phonon polarization vectors are independent of the magnitude of the phonon wave vector, equation (1) can be written

$$J(\mathbf{H}) = \frac{Nf^2\exp(-2M)}{(v/n)}\,k_BT\left[\frac{1}{S(g)}\right]^2\frac{1}{|\mathbf{g}|^2}\sum_j\frac{(\mathbf{H}\cdot\mathbf{e}_{gj})^2}{\varrho V_{gj}^2}, \tag{3}$$

where ϱ is the density of the crystal and where the phonon velocities and polarization vectors are those for the long-wavelength phonons with wave vector parallel to $\mathbf{g}$.

For crystals of cubic symmetry equation (3) can be manipulated into an alternative form (see Waller, 1925; Nilsson, 1957) that avoids the need for explicit evaluation of the phonon polarization vectors and velocities and thus is more amenable to calculations. Let us introduce dimensionless vector components and ratios of elastic constant combinations through the relations

$$\begin{aligned} \mathbf{H} &= h_1\mathbf{a}_1^* + h_2\mathbf{a}_2^* + h_3\mathbf{a}_3^* \\ \mathbf{g} &= g_1\mathbf{a}_1^* + g_2\mathbf{a}_2^* + g_3\mathbf{a}_3^* \\ H^2 &= h_1^2 + h_2^2 + h_3^2 \\ g^2 &= g_1^2 + g_2^2 + g_3^2 \\ x_1 &= (C_{11} - C_{12} - 2C_{44})/C_{44} \\ x_2 &= x_1(C_{11} + C_{12})/C_{11} \\ x_3 &= x_1^2(C_{11} + 2C_{12} + C_{44})/C_{11} \\ x_4 &= (C_{12} + C_{44})/C_{11} \\ x_5 &= (C_{11} - C_{44})/C_{11}, \end{aligned} \tag{4}$$

the $\mathbf{a}^*$ being the axes of the cubic unit cell in reciprocal space. Equation (3) can then be written

$$J(\mathbf{H}) = \frac{Nf^2\exp(-2M)}{(v/n)}\,k_BT\left[\frac{1}{S(g)}\right]^2\frac{C(\mathbf{H},\mathbf{g})}{D(\mathbf{g})} \tag{5}$$

where

$$C(\mathbf{H},\mathbf{g}) = \frac{1}{C_{44}}\left\{\begin{array}{l} H^2g^4 - x_5g^2(h_1^2g_1^2 + h_2^2g_2^2 + h_3^2g_3^2) \\ +x_2(h_1^2g_2^2g_3^2 + h_2^2g_3^2g_1^2 + h_3^2g_1^2g_2^2) \\ -2x_4\left[\begin{array}{l} h_1h_2g_1g_2(x_1g_3^2 + g^2) + h_2h_3g_2 \\ \times g_3(x_1g_1^2 + g^2) + h_3h_1g_3g_1 \\ \times(x_1g_2^2 + g^2) \end{array}\right] \end{array}\right\} \tag{6}$$

and

$$D(\mathbf{g}) = g^6 + x_2g^2(g_1^2g_2^2 + g_2^2g_3^2 + g_3^2g_1^2) + x_3g_1^2g_2^2g_3^2\,. \tag{7}$$

If the crystal is elastically isotropic, $x_1=x_2=x_3=0$ and $x_4=x_5$ and equations (5)–(7) yield the intensity relation for Suortti's model.

The intensity expression for Warren's much simpler model (one velocity for all phonons) is obtained by setting $S(g)=1$ and replacing the ratio, $C(\mathbf{H},\mathbf{g})/D(\mathbf{g})$, by its average over all orientations of $\mathbf{g}$ (with fixed $\mathbf{H}$),

$$\left\langle\frac{C(\mathbf{H},\mathbf{g})}{D(\mathbf{g})}\right\rangle = \frac{\mathscr{K}}{3}\frac{H^2}{g^2} \tag{8}$$

where the velocity factor, $\mathscr{K}$, is evaluated in various ways (Nilsson, 1957; Walker & Chipman, 1969). For elastic isotropy,

$$\mathscr{K} = 1/C_{11} + 2/C_{44}\,.$$

We now average equation (5) over all orientations of $\mathbf{H}$ to obtain the one-phonon TDS intensity for a powder pattern. This average will include contributions from points in Brillouin zones around a number of non-equivalent reciprocal lattice points, each weighted by its multiplicity. Let the position of $\mathbf{H}$ in the Brillouin zone around the reciprocal lattice point given by $\boldsymbol{\tau}_j$ be specified by a polar angle ψ, measured from $\boldsymbol{\tau}_j$, and an azimuthal angle φ with arbitrary zero. The maximum angle, ψ_{mj}, for $\mathbf{H}$ at the boundary of the spherical Brillouin zone, is determined by

$$g_m^2 = H^2 + \tau^2 - 2H\tau\cos\psi_{mj},$$

where $\tau=a|\boldsymbol{\tau}|$, dimensionless. The one-phonon TDS intensity for a powder pattern is then given by

$$J(H) = \frac{Nf^2\exp(-2M)}{(v/n)}\,\frac{k_BT}{4\pi}\sum_j p_jI_j(H) \tag{9}$$

where

$$I_j(H) = \int_0^{\psi_{mJ}}\int_0^{2\pi}\left[\frac{1}{S(g)}\right]^2\frac{C(\mathbf{H},\mathbf{g})}{D(\mathbf{g})}\sin\psi\,\mathrm{d}\psi\mathrm{d}\varphi \tag{10}$$

and where the sum is over the different reciprocal lattice points, of multiplicity p_j, whose Brillouin zones are intercepted by the sphere of radius H.

The Debye–Waller exponent for a monatomic cubic sample can be written

$$2M = \frac{k_BT}{Nm}\sum_{gj}\frac{(\mathbf{H}\cdot\mathbf{e}_{gj})^2}{v_{gj}^2}$$

where the sum is over all phonons. By making the same

approximations as above and changing the sum over wave vectors to an integration, this can be evaluated as

$$2M = \frac{k_B T}{(v/n)} \frac{H^2}{g_m^2} 1{\cdot}3862\mathscr{K} \tag{11}$$

where

$$\frac{1}{g_m}\int_0^{g_m}\left[\frac{1}{S(g)}\right]^2 \mathrm{d}g = 1{\cdot}3862\,.$$

Then by combining equations (9) and (11) one can write

$$\frac{J(H)}{Nf^2\exp(-2M)\,2M} = \frac{g_m^2}{1{\cdot}3862\mathscr{K}}\frac{1}{4\pi H^2}\sum p_j I_j(H)\,. \tag{12}$$

The normalized intensity of equation (12), denoted C_1 in most studies, is a convenient quantity for comparing predictions for different materials or different models, since factors that only alter the intensity $J(H)$ by a constant multiplier are canceled. Thus this normalized intensity for anisotropic materials may depend on the ratios of the elastic constants but not on their magnitudes, while the actual intensity $J(H)$ of course does depend on these values.

We have used equation (12) to calculate the normalized TDS intensity distribution for body-centered cubic samples with three quite different sets of elastic constants,* illustrating (*a*) almost perfect isotropy (anisotropy factor $\mathrm{AF}=2C_{44}/(C_{11}-C_{12})=1{\cdot}008$); (*b*) large anisotropy favoring (110) shear (AF=9·21), and (*c*) large anisotropy favoring (100) shear (AF=0·254). The results are given by the three curves of normalized intensity as a function of H plotted in Fig. 1. The curves all show sharp peaks at the positions of the powder pattern reflections, but the feature to be noted is that the curves for the anisotropic cases show appreciable systematic differences from the curve for the isotropic case, with the effects for the case with $\mathrm{AF}>1$ generally being opposite in sign to those for $\mathrm{AF}<1$. Elastic anisotropy thus can still produce significant effects despite the powder pattern averaging. It should be added that our cases (*b*) and (*c*) represent cases of rather extreme anisotropy and that most materials, being less anisotropic, will show smaller effects.

It is of interest to compare our results for the isotropic case with the corresponding results from previous approaches. Suortti's model gives the same results as ours, since the two models do not differ in the case of isotropy. The two-velocity model of Paskin (1959) neglects dispersion, causing the calculated $2M$ to be smaller than our value [equation (11)] by the ratio, 1:1·386, and its normalized intensity for values of H beyond the first reflection is larger than our results near reflections (theoretically, by 38·6% at the singularity) and smaller than our results near the minima between reflections (by as much as 15%, between the first two reflections). The model of Warren (1953) neglects dispersion and also assumes that longitudinal and transverse phonons have the same velocity; the effects of these two approximations largely counteract one another here, and the normalized intensity distribution for values of H beyond the first reflection differs from our curve by 6·6% at the singularities and by only ±5% or less near the minima. Then, because of the smaller value of $2M$, the 'actual' intensities $J(H)$ for the Paskin and Warren models will be reduced further by the factor, 1/1·386, compared to ours, unless a common value of $2M$ is used in all calculations.

* The data are for (*a*) tungsten, (*b*) β-CuZn, and (*c*) RbI.

Included TDS correction

Theory

The scattered power from a polycrystalline specimen (neglecting absorption) entering a fixed rectangular detector slit can be written

$$P = I_e L W \int z(H)J(H)\mathrm{d}H \tag{13}$$

where $J(H)$ is the intensity in electron units of the scattering under consideration; H is the dimensionless reciprocal space variable introduced earlier, given by $H=(2a\sin\theta)/\lambda$, where 2θ is the scattering angle and λ is the wavelength; I_e is the electron unit; L and W are the slit length and width respectively; and $z(H)$ is the resolution function of the experiment, a function of the mean scattering angle of the receiver slit and the instrumental divergences and wavelength distribution, normalized so that

$$\int z(H)\mathrm{d}H = 1\,.$$

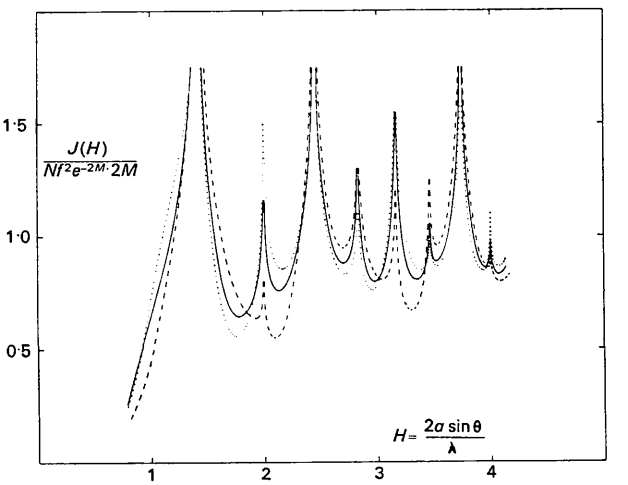

Fig. 1. The normalized TDS intensity distribution for powder patterns of monatomic b.c.c. materials. The radial reciprocal space variable H has the value, 2, at the position of the 200 reflection. The solid curve is for an elastically isotropic material (AF=1·01), the dashed curve is for a very anisotropic material with easy (110) shear (AF=9·21), and the dotted curve is for a very anisotropic material with easy (100) shear (AF=0·25).

To simplify calculations, we shall assume that the wavelength distribution of the primary beam is the dominant factor in the resolution function and neglect the effects of other factors such as beam divergences and receiver slit dimensions. Equation (13) then becomes

$$P=I_eLW\sum_i w_iJ(H_i) \tag{14}$$

where w_i is the weight of the ith wavelength component λ_i, normalized so that

$$\sum_i w_i=1\,,$$

and $H_i=(2a\sin\theta)/\lambda_i$, where 2θ is the mean scattering angle for the detector slit.

Consider now the integrated scattering, E, measured when the detector moves with constant angular velocity 2ω in a scan from $2\theta_1$ to $2\theta_2$ which takes it through the powder pattern reflection, $H=\tau=(h^2+k^2+l^2)^{1/2}$, where h, k, and l are the reflection indices. We assume that this scan is short enough and the wavelength spread small enough for the rate of change of the variables H_i to be treated as constant throughout the scan and as independent of wavelength, *i.e.* $\dot{H}_i=\dot{H}=\omega(2a\cos\theta)/\lambda$, where θ and λ are average values. We then can write

$$\begin{aligned}E&=\int P\mathrm{d}t\\&=\frac{I_eLW}{\dot{H}}\sum_i w_i\int_{H_{1i}}^{H_{2i}}J(H)\mathrm{d}H,\end{aligned} \tag{15}$$

where $H_{1i}=(2a\sin\theta_1)/\lambda_i$, and where we have chosen $\theta_2>\theta_1$.

The intensity function $J_B(H)$ for the Bragg powder pattern reflection is given by

$$J_B(H)=\frac{N'|\bar{F}|^2p}{4\pi\tau^2}\,\delta(\tau-H), \tag{16}$$

where N' is the number of unit cells in the sample; $\bar{F}$ and p are the average structure factor and the multiplicity of the reflection respectively; $\tau^2=h^2+k^2+l^2$ for that reflection; and the delta-function is normalized so that

$$\int\delta(\tau-H)\mathrm{d}H=1\,.$$

The integrated intensity of the Bragg powder pattern reflection measured during this scan is then obtained from equations (15) and (16) as

$$E_B=\frac{I_eLW}{\dot{H}}\frac{N'|\bar{F}|^2p}{4\pi\tau^2} \tag{17}$$

which is consistent with the usual expression (James, 1948).

The integrated diffuse scattering measured during the scan can then be obtained from equations (15) and (17) as

$$E_D=E_B\frac{4\pi\tau^2}{N'|\bar{F}|^2p}\sum_i w_i\int_{H_{1i}}^{H_{2i}}J_D(H)\mathrm{d}H \tag{18}$$

where $J_D(H)$ is the intensity function for the diffuse scattering.

A weighted background often subtracted from such a measurement is obtained by multiplying the average of the background power at the ends of the scan by the scan time, $(H_{2i}-H_{1i})/\dot{H}=(H_2-H_1)/\dot{H}$. From equations (14) and (17) this can be written

$$E_D'=E_B\frac{4\pi\tau^2}{N'|\bar{F}|^2p}(H_2-H_1)\sum_i w_i\{J_D(H_{1i})+J_D(H_{2i})\}/2. \tag{19}$$

We now confine our attention to one-phonon TDS, using the intensity function given by equation (9). Then, noting that for small scans

$$\frac{Nf^2\exp(-2M)}{(v/n)}\simeq\frac{N'|\bar{F}|^2}{v}\,,$$

equations (18) and (19) give

$$\frac{E_D}{E_B}=\alpha_1=\frac{k_BT}{v}\frac{\tau^2}{p}\sum_i w_i\int_{H_{1i}}^{H_{2i}}\sum_j p_jI_j(H)\mathrm{d}H \tag{20}$$

and

$$\begin{aligned}\frac{E_D'}{E_B}=\alpha_1'&=\frac{k_BT}{v}\frac{\tau^2}{p}(H_2-H_1)\\&\quad\times\sum_i w_i\sum_j p_j\{I_j(H_{1i})+I_j(H_{2i})\}/2\end{aligned} \tag{21}$$

and the background-corrected, 'measured' integrated intensity, E_M, is related to the integrated intensity of the Bragg powder pattern reflection, E_B, by

$$\begin{aligned}E_M&=E_B(1+\alpha_1-\alpha_1')\\&=E_B(1+\alpha)\,.\end{aligned} \tag{22}$$

The function $I_j(H)$ [equation (10)] has a singularity at $\mathbf{g}=0$ which requires special treatment in a numerical integration of equation (20). Our procedure, following the method shown in the section, *Theory* 2, of Walker & Chipman (1970), has been to transform that part of the integral through a small volume enclosing the reciprocal lattice point bounded by sections of conical (constant ψ) or spherical (constant H) surfaces into an integral over the surface of that volume, writing

$$\begin{aligned}&\iiint\left[\frac{1}{S(g)}\right]^2\frac{C(\mathbf{H},\mathbf{g})}{D(\mathbf{g})}\sin\psi\mathrm{d}H\mathrm{d}\psi\mathrm{d}\varphi\\&\qquad=\iint_{\mathscr{S}}\left[\frac{1}{S(g)}\right]^2\frac{C(\mathbf{H},\mathbf{g})}{D(\mathbf{g})}\frac{1}{H^2}g_n\mathrm{d}A\end{aligned} \tag{23}$$

where $\mathscr{S}$ denotes the surface of that small volume, and g_n is the component of g perpendicular to the differential area, dA. Evaluation of the surface integrals and the remaining volume integration of equation (20) is then straightforward.

Calculation

We have developed a computer program to calculate the included TDS correction α on the basis of the methods and equations of the preceeding sections. The program, called *PTDS2*, is written in FORTRAN IV and is described in detail elsewhere (Walker & Chipman, 1972*a*). It involves a three-dimensional numerical integration [equations (20), (21) and (23) combined] over the segment of the Brillouin zone around each nonequivalent reciprocal lattice point that is intercepted in a given scan. Using this program, with integration parameters chosen to yield results accurate generally to 1% or better, we have carried out calculations to investigate the dependence of this correction on a number of factors.

Let us consider first the results obtained for an elastically isotropic sample, tungsten. We acknowledge that many of the conclusions to be drawn from these calculations were pointed out previously by Suortti from his isotropic model calculations. However, Suortti's work is apparently not widely known, judging from the continued use of poor approximations in several recent papers, and our calculations are more extensive and systematic than his, so our calculations and conclusions are given here to illustrate and amplify the results for an isotropic case before we consider the further effects of anisotropy.

We have calculated the TDS correction α for a series of reflections from tungsten at 300°K using a single wavelength, $\lambda = 0{\cdot}71140$ Å (midway between the wavelengths of Mo $K\alpha_1$ and Mo $K\alpha_2$), and a symmetrical scan through each reflection with $2\theta_2 - 2\theta_1 = \Delta 2\theta = 2{\cdot}5°$ (which includes 0·4 of the range to adjacent reflections for the closest group of lines). The results are plotted as the solid points in Fig. 2(*a*) as a function of the sum of the squares of the indices of the reflection. The vertical bar drawn from the horizontal axis at each value of $\tau^2 = h^2+k^2+l^2$ has a length proportional to the multiplicity of that reflection. The values of α show large variations with increasing τ^2, with the value for the 444 reflection being negative, and there is a strong correlation between the relative sizes of the values of α for adjacent reflections and the relative multiplicities of those reflections. The small size of the corrections is caused by the unusually strong elastic constants of tungsten.

To test the sensitivity of the calculation to the approximations in our model, we have repeated this calculation for two alternate dispersion approximations, in case (0) putting $S(g)$ equal to unity (no dispersion, reducing $2M$ by 1/1·386), and in case (2) replacing $S(g)$ by $[S(g)]^2$ (greater dispersion, increasing $2M$ by 1·502). The relative change in a value of α resulting from using case (0) was only $\pm 3{\cdot}6\%$ or less for 23 of the 27 reflections and was only $\pm 5{\cdot}8\%$ or less for these same reflections on using case (2). [The reflections with $\tau^2 = 12$, 16, 32, and 48, all of low multiplicity compared to neighboring reflections, showed changes in α of 4·8, −2·4, 12·0 and 7·6% respectively for case (0) and changes of −13·2, 10·4, −27·0 and −20·6% for case (2).] A comparison with case (0) was also made for a shorter scan, $\Delta 2\theta = 1{\cdot}0°$, which showed a maximum difference in α for any reflection of only $\pm 1{\cdot}2\%$. Since cases (0) and (2) correspond to quite large changes in the shorter-wavelength phonons, it is clear from these results that the characteristics of the long-wavelength phonons must dominate the calculation of α. The limitations of the spherical Brillouin zone approximation and the assumptions concerning phonon dispersion and polarization in our model affect only the shorter-wavelength phonons, so the error in α due to these approximations thus generally should be quite small.

To investigate the effects of instrumental factors, we have repeated the original calculation, replacing the single wavelength by the two wavelengths, Mo $K\alpha_1$ and Mo $K\alpha_2$, with weights of $\frac{2}{3}$ and $\frac{1}{3}$ respectively, which gives a reasonable first approximation to a real Mo $K\alpha$ doublet. The percentage change in the value of α caused by the change to this wavelength doublet is plotted for the various reflections in Fig. 2(*b*). There

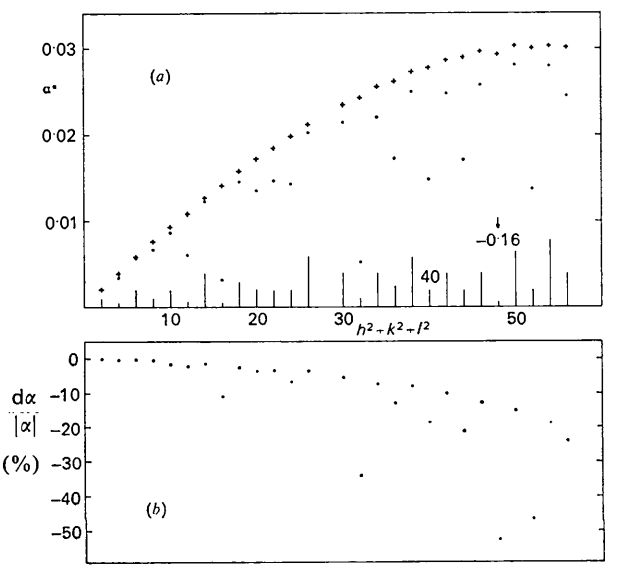

Fig. 2. (*a*) The included TDS correction for reflections from an isotropic b.c.c. material, tungsten, at 300°K measured with symmetrical scans and a mean Mo $K\alpha$ single wavelength, as a function of the sum of the squares of the indices of the reflections. The solid points display $\alpha^* = \alpha$ for a scan length, $\Delta 2\theta = 2{\cdot}5°$. The crosses display $\alpha^* = 5\alpha$ for a scan length, $\Delta 2\theta = 0{\cdot}5°$. The vertical line drawn from the horizontal axis at each value of $h^2+k^2+l^2$ has a length proportional to the multiplicity of that reflection. (*b*) The percentage change in the values of α for the 2·5° scan when the single mean wavelength is replaced by the appropriately weighted two wavelengths of Mo $K\alpha_1$ and Mo $K\alpha_2$.

is a reduction in the value of α for each reflection (the value for 444 becoming more negative) which increases overall with increasing τ^2, and the reduction is greater for the reflections of low multiplicity, particularly those adjacent to reflections of high multiplicity. The change is 10% or more for 12 of these 27 reflections, and ranges up to 53% for the 444 reflection. This 'instrumental' effect varies with the length of the scan; a repeat of these calculations for a scan length, $\Delta 2\theta = 2{\cdot}0°$, shows the percentage reduction in α due to the change to this wavelength doublet to be larger for the 2·0° scan than for the previous 2·5° scan for 21 of the 27 reflections. The effect seems generally large enough for it not to be neglected where accurate corrections are required.

Next we have investigated the dependence of α on the length of the scan by repeating the original calculation for values of $\Delta 2\theta$ ranging from 0·5 to 3·0°. The 0·5° scan is too short to be practical for most real experiments, but it is useful in indicating the behavior of the TDS correction in the limit of very short scans. The results for this 0·5° scan are given by the crosses in Fig. 2(*a*), where we have plotted 5α, *not* α, in order to facilitate comparison with the values of α for the 2·5° scan. The values of 5α for this short scan show an almost smooth monotonic dependence on τ^2, with only small reductions for the low multiplitiy reflections. A comparison of these values of 5α with the corresponding values of α for the 2·5° scan shows that α has not varied linearly with $\Delta 2\theta$ for any reflection, with quite large differences for some low multiplicity reflections but only small differences for a few high multiplicity reflections. The non-linearity increases with increasing $\Delta 2\theta$ at a rate dependent on the relative multiplicities of neighboring reflections, so that for $\Delta 2\theta = 2{\cdot}5°$, the derivative, $\mathrm{d}\alpha/\mathrm{d}(\Delta 2\theta)$, has become negative for six reflections ($\tau^2 = 12$, 16, 32, 40, 48, and 52). This non-linearity is due to the contributions to α from the intercepted segments of Brillouin zones around all other reciprocal lattice points except those for the reflection being measured, these 'other' contributions being negligible for very small scans but increasing approximately as $(\Delta 2\theta)^3$ and generally being negative.

Chipman & Paskin (1959*b*) derived an expression for the included TDS in symmetrical powder pattern scans based on Warren's model that has subsequently been widely used. In our nomenclature their expression can be written

$$\alpha_{\mathrm{CP}} = \frac{k_B T}{v}\frac{2\pi\mathscr{K}}{3}\tau^2(H_2 - H_1) \propto \tau^2 \cos\theta \Delta 2\theta \qquad (24)$$

where there has been some controversy (see Borie, 1961) over the value of the proportionality constant that should be used. Regardless of that question, equation (24) predicts that the correction varies smoothly as $\tau^2 \cos\theta$ for constant $\Delta 2\theta$ and depends linearly on $\Delta 2\theta$, while our results show that neither of these predictions is usually satisfied for reasonable scan lengths. It thus must be emphasized that the Chipman–Paskin relation is a poor approximation which can be appreciably in error for normal experimental conditions, even when the material is elastically isotropic.

Now, to examine the effects of elastic anisotropy, we have calculated the TDS correction for the same series of reflections from a very anisotropic b.c.c. sample (data are for β-CuZn, with AF = 9·21) for the same single wavelength and temperature and for symmetrical scans of two lengths, $\Delta 2\theta = 0{\cdot}5$ and 2·5°. The results for the 0·5° scan are shown by the crosses in Fig. 3, where again we have plotted 5α, *not* α, to facilitate comparison with the values of α for the 2·5° scan, and where adjacent points have been linked with straight line segments to make the results more visible. In contrast to the almost smooth monotonic dependence of the isotropic sample short-scan data, these values for the anisotropic sample show quite large variations as a function of τ^2, with plus and minus departures from the average curve ranging up to a factor of two. The Chipman–Paskin relation [equation (24)] clearly is a poor approximation for this anisotropic sample even in the limit of small scans.

The values of α for the 2·5° scan of the reflections from this sample are given by the solid points in Fig. 3. A comparison with the data for the 0·5° scan shows again that α does not generally vary linearly with $\Delta 2\theta$, with large differences for some reflections and only small differences for others. This non-linearity differs from that for the isotropic sample in several instances (*e.g.* the 444 and 400 reflections) as a result of the effects of the different anisotropic TDS distributions around neighboring reciprocal lattice points as well as their relative multiplicities. The substantial size of these values of α should also be noted.

Approximation

The method of evaluating the correction α presented in the preceding sections seems capable of yielding an accuracy of 1% or better for a wide variety of conditions, but it can require an appreciable amount of time on a high-speed computer. For example, the 2·5° scan data for the isotropic sample shown in Fig. 2(*a*) took an average of 6·5 seconds of CDC-6400 computing time per reflection, while the 2·5° scan data for the anisotropic sample given in Fig. 3 took approximately 26 seconds per reflection because of the finer mesh needed with such anisotropy. We have thus looked for a simpler approach that would allow a considerable reduction in computation requirements where a moderate loss in accuracy could be accepted.

We consider the simple Warren model for the elastic vibrations, but with one modification: The velocity factor to be used for all the phonons in a Brillouin zone is determined by a circular average over those long-wavelength phonons whose wave vector **g** is perpendicular to the reciprocal lattice vector to the center

of that Brillouin zone, rather than by a spherical average over all orientations of **g**. The factor $\mathscr{K}$ in equation (8) is then replaced by K_j, where

$$\left\langle \frac{C(\tau_j,\mathbf{g})}{D(\mathbf{g})} \right\rangle_{\mathbf{g}\perp\tau_j} = \frac{K_j}{3}\frac{\tau_j^2}{g^2} . \qquad (25)$$

This modification has two major consequences; (*a*) the average involves mainly a set of 'transverse' modes, and (*b*) if the crystal is elastically anisotropic, the velocity factor K_j can be different for phonons in zones around different reciprocal lattice points. The values of K_j for general reciprocal lattice points for an anisotropic cubic crystal can be obtained numerically from equations (6) and (7). For *h*00 reciprocal lattice points and arbitrary anisotropy (and thus for all reciprocal lattice points in the case of elastic isotropy)

$$K_{h00}=3/C_{44} .$$

Equation (10) is readily evaluated for this modified Warren (*W'*) model, giving

$$I_j(H)=\frac{2\pi K_j}{3}\frac{H}{\tau_j}\ln\left(\frac{g_m}{|H-\tau_j|}\right) . \qquad (26)$$

The TDS correction is now obtained from equations (20)–(22) with equation (26). The evaluation of equation (20) involves only standard integrals with no further approximations. After some manipulations the result for a single wavelength can be written

$$\alpha_{W'}=\frac{k_BT}{v}\frac{\pi}{3}\tau_0\sum_j K_j\left(\frac{p}{\tau}\right)_j\left(\frac{\tau}{p}\right)_0 \times\left\{\begin{array}{l}(\varepsilon_2+\varepsilon_1)(\tau_0+\tau_j)+(\varepsilon_2^2-\varepsilon_1^2)/2 \\ -(H_1H_2-\tau_j^2)\ln\left|\dfrac{\tau_0-\tau_j+\varepsilon_2}{\tau_0-\tau_j-\varepsilon_1}\right|\end{array}\right\} \qquad (27)$$

where the sum is over the non-equivalent reciprocal lattice points for which $(H_1-g_m)\le\tau_j\le(H_2+g_m)$; where $\varepsilon_1=(\tau_0-H_1)$ and $\varepsilon_2=(H_2-\tau_0)$, except that if $(H_1-g_m)\le\tau_j\le(H_2-g_m)$, then $\varepsilon_2=g_m-(\tau_0-\tau_j)$, or if $(H_1+g_m)\le\tau_j\le(H_2+g_m)$, then $\varepsilon_1=g_m+(\tau_0-\tau_j)$; and where the subscript 0 indicates a value for the reflection being scanned. The result for multiple wavelengths is then obtained by evaluating equation (27) in turn with the values of H_1 and H_2 for each wavelength and summing the results with the appropriate weights.

Equation (27) reduces to the Chipman–Paskin relation, equation (24), if the scan is symmetrical (*i.e.* $\varepsilon_1=\varepsilon_2$), if one neglects the terms from all other reciprocal lattice points except those being scanned (those with $\tau_j=\tau_0$), and if the differences between the various K_j and $\mathscr{K}$ are ignored.

We have developed a computer program to calculate the various velocity factors K_j and the correction α_W' according to the above equations. The program, called *PTDS*3, is written in FORTRAN IV and is described in detail elsewhere (Walker & Chipman, 1972*b*). It first evaluates any unknown K_j's for a given set of reciprocal lattice points and then uses these in calculating $\alpha_{W'}$ for each of the desired series of scans. When used on a CDC-6400 computer, it required 0·1 seconds to calculate K_j for a set of 46 reciprocal lattice points and it then used an average of 0·01 seconds per case to calculate $\alpha_{W'}$ for various scans of the 27 b.c.c. reflections studied previously. This represents a gain in speed of two to three orders of magnitude over the first program, *PTDS*2.

Let us now compare the values of $\alpha_{W'}$ from this simple approach with the corresponding values of α from the previous, more sophisticated calculations made with the program, *PTDS*2. For the short, 0·5° scans there is good agreement for both the isotropic and the anisotropic samples, the largest differences being 2·6% for the isotropic 444 reflection and 3·2% for the anisotropic 400 reflection. As the scan length increases the differences generally increase somewhat, but they remain surprisingly small overall, with the largest differences occurring for reflections of low multiplicity adjacent to reflections of high multiplicity. For the isotropic sample the largest difference, $\alpha_{W'}-\alpha$, (that for the 444 reflection) varies smoothly from $-0{\cdot}0002$ for $\Delta 2\theta=0{\cdot}5°$ to $-0{\cdot}0018$ for $\Delta 2\theta=2{\cdot}5°$, while the smaller differences for the other reflections for this range of scans never exceed 5% of the value of α. For the anisotropic sample the largest difference (that for the 400 reflection) increases from $-0{\cdot}0002$

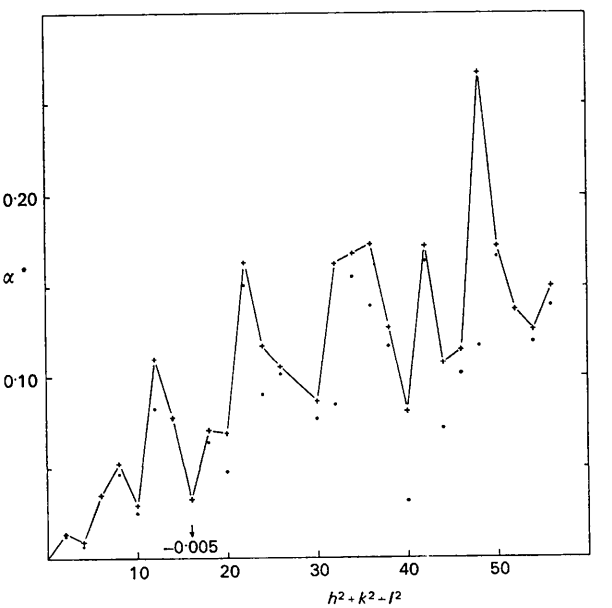

Fig. 3. The included TDS correction for reflections from a very anisotropic b.c.c. material (data are for β-CuZn) at 300°K measured with symmetrical scans and a mean Mo *Kα* single wavelength, as a function of the sum of the squares of the indices of the reflections. The solid points display $\alpha^*=\alpha$ for a scan length, $\Delta 2\theta=2{\cdot}5°$. The crosses display $\alpha^*=5\alpha$ for a scan length, $\Delta 2\theta=0{\cdot}5°$. The crosses have been linked with line segments to make the large variations in α more visible.

for $\Delta 2\theta = 0{\cdot}5°$ to $-0{\cdot}0082$ for $\Delta 2\theta = 2{\cdot}5°$, while the smaller differences for all except one of the other reflections for $\Delta 2\theta = 2{\cdot}5°$ are less than 9% of the value of α, the exception being the 110 reflection, where the difference of 0·0019 is 16% of the value of α.

Thus this W' model, despite its unrealistic assumptions, is able to yield reasonably accurate values for the included TDS correction with small computation times for a considerable range of scans even for samples with rather extreme anisotropy, so it should prove to be a useful approximation for many cases.

Discussion

The present study was undertaken to develop a method for calculating the thermal diffuse scattering in powder patterns that would improve on previous approaches by employing a correct description of the frequencies and polarization vectors of the long-wavelength phonons for materials of arbitrary elastic anisotropy. The approximations used in treating the shorter-wavelength phonons – linear chain dispersion; wavelength-independent polarization vectors; spherical Brillouin zone – are the same as those of the best previous model (Suortti, 1967) and are thought not to be sources of significant error. The method has been limited to monatomic cubic crystals, to one-phonon scattering, to temperatures of the order of the Debye temperature or higher, and to scattering angles not much smaller than that of the first reflection, and it is more accurate for X-ray scattering than for neutron scattering, where further approximations are required.

The theory for our approach, given in the first two sections, is a relatively straightforward adaptation of single crystal TDS relations (see, for example, Walker & Chipman, 1970) to powder pattern conditions, with no particularly novel features. We evaluate these equations by numerical calculations on a high speed computer. The results obtained are estimated to be generally rather accurate (*e.g.* 1% or better for an included TDS correction), but the approach can be costly in its computing time requirements because of the complexity of the equations and the density of points needed in the integrals.

Using this approach, we have made a number of calculations to investigate both the TDS intensity distribution in a powder pattern and the correction for included TDS in the measured integrated intensities of powder lines. The calculations were carried out for a b.c.c. lattice, but the general conclusions are expected to be valid also for other lattices. These conclusions are:

(1) Despite the powder pattern averaging, elastic anisotropy in a lattice can produce marked differences both in the TDS intensity distribution and in the included TDS correction.

(2) The included TDS correction is generally quite insensitive to large changes in the characteristics of the shorter wavelength phonons, while the TDS intensity distribution of course does reflect such changes, the effects being most noticeable at angles away from the reflections.

(3) The included TDS correction generally should not be expected to vary smoothly with τ^2 or linearly with the length of scan, even for isotropic samples. The Chipman–Paskin approximation, which predicts such smoothness and such linearity, can be greatly in error for reasonable experimental conditions.

(4) Instrumental factors such as a doublet wavelength distribution can produce significant changes in the included TDS correction, particularly for weak reflections adjacent to strong reflections, which display the most sensitive response to the various factors in the calculation.

Suortti reached essentially the same conclusions as in (2)–(4) above, except that he found the instrumental effects to be somewhat less important.

We have also developed a much simpler method for calculating the included TDS correction that is two to three orders of magnitude faster than our major approach at the expense of only a moderate loss in accuracy. The method uses Warren's one-velocity phonon model, modified by specifying that the velocity associated with the phonons in the zone around a given reciprocal lattice point is to be determined from an average of the correct factor for those long-wavelength phonons contributing to the scattering in the plane perpendicular to that particular reciprocal lattice vector. This modification both gives a larger mean value for the velocity factor K (and hence the TDS intensity) than that from the usual spherical average and it also allows the velocity factor to differ for different reciprocal lattice points when there is elastic anisotropy; for example, the values of K_j differ by as much as a factor of 4·3 for the very anisotropic case we have considered. This W' model of course gives a quite unrealistic description of individual phonons, but apparently it does contain those features that are important for a calculation of the included TDS correction for powders, since we find that it gives relatively accurate values for most reflections and reasonable lengths of scan even for very anisotropic materials.

Our study was limited to temperatures of the order of the Debye temperature or higher. We suggest, however, that the calculation of the included TDS correction should be valid down to much lower temperatures than this because of its insensitivity to changes affecting the shorter wavelength phonons, although the calculation of the TDS intensity distribution still faces this restriction. Our study was also limited to monatomic cubic materials. An approximate extension to polyatomic cubic materials can be obtained, following Suortti, by ignoring optic modes and weighting the intensity contribution from acoustic phonons in the zone around a particular reciprocal lattice point by the square of the structure factor of that Bragg reflection, as well as its multiplicity, in place of the common squared structure factor multiplier

given in equation (9). While this should offer a reasonable first approximation for the included TDS correction (but not the intensity distribution), its accuracy for weaker reflections and normal scans is open to serious question when there are appreciable differences between neighboring structure factors (such as in NaCl, for example) because of the uncertainty in any large negative contributions from 'other' reciprocal lattice points. An extension to non-cubic materials should also be possible using the relations derived by Rouse & Cooper (1969), but the results should be considerably more complicated. Finally, our study was also limited to one-phonon scattering. Calculations based on simple models (Paskin, 1959; Borie, 1961) show that the neglected n-phonon TDS varies as $(2M)^n/n!$ so our calculated intensity distribution can give a good estimate of the total TDS only if $2M$ is small. The two-phonon and higher order TDS distributions appear to peak much less sharply than does the one-phonon TDS, so their contribution to an included TDS correction should be much smaller, but there has not yet been any specific calculation of these quantities. Thus, if the one-phonon included TDS correction is large, the neglect of the higher-order terms must be recognized to be a possible significant source of error.

References

BORIE, B. (1961). *Acta Cryst.* **14**, 566.
CHIPMAN, D. R. & PASKIN, A. (1959*a*). *J. Appl. Phys.* **30**, 1992.
CHIPMAN, D. R. & PASKIN, A. (1959*b*). *J. Appl. Phys.* **30**, 1998.
COCHRAN, W. (1963). *Rep. Progr. Phys.* **26**, 1.
HERBSTEIN, F. H. & AVERBACH, B. L. (1955). *Acta Cryst.* **8**, 843.
JAMES, R. W. (1948). *The Optical Principles of the Diffraction of X-rays*. London: Bell.
NILSSON, N. (1957). *Ark. Fys.* **12**, 247.
PASKIN, A. (1958). *Acta Cryst.* **11**, 165.
PASKIN, A. (1959). *Acta Cryst.* **12**, 290.
ROUSE, K. D. & COOPER, M. J. (1969). *Acta Cryst.* A**25**, 615.
SCHOENING, F. R. L. (1969). *Acta Cryst.* A**25**, 484.
SUORTTI, P. (1967). *Ann. Acad. Sci. Fenn. Ser. A*, **VI**, 240.
WALKER, C. B. & CHIPMAN, D. R. (1969). *Acta Cryst.* A**25**, 395.
WALKER, C. B. & CHIPMAN, D. R. (1970). *Acta Cryst.* A**26**, 447.
WALKER, C. B. & CHIPMAN, D. R. (1972*a*). Report AMMRC TR 72-27.
WALKER, C. B. & CHIPMAN, D. R. (1972*b*). Report AMMRC TR 72-28.
WALLER, I. (1925). Dissertation, Uppsala.
WARREN, B. E. (1953). *Acta Cryst.* **6**, 803.
WILLIS, B. T. M. (1969). *Acta Cryst.* A**25**, 277.

Acta Cryst. (1972). A**28**, 580

Application of Representation Analysis to the Magnetic Structure of Nickel Chromite Spinel

BY E. F. BERTAUT AND J. DULAC

C.N.R.S. and C.E.N.-G – Grenoble, France

(*Received* 24 *April* 1972)

The magnetic structure of the tetragonal nickel chromite spinel ($a_0=5{\cdot}76$; $c=8{\cdot}50$ Å) has been solved by representation analysis in space group $I4_1/amd$. Magnetic reflexions decompose into two sets; (*a*) ferrimagnetic ones, produced by a Néel mode along the x-axis and belonging to the two-dimensional Γ_{5g} representation of wave vector $\mathbf{k}=[000]$; (*b*) antiferromagnetic reflexions produced by non-colinear anticentered y and z modes belonging to a two-dimensional representation of wave vector $\mathbf{k}=[001]$. The Shubnikov groups of the ferri- and antiferromagnetic modes considered separately are $Imm'a'$ and $I_p2'2'2_1$ respectively. Their intersection has the very low symmetry $P2'_y$. The antiferromagnetic mode of Ni (in 000 and $0\frac{1}{2}\frac{1}{4}$) has only y components ($S_y=0{\cdot}58$). The chromium spins decompose into two sets: Cr_I (in $0\frac{1}{4}\frac{5}{8}$ and $\frac{1}{2}\frac{1}{4}\frac{1}{8}$) has y and z components ($S_y=+0{\cdot}73$ for the former and $-0{\cdot}73$ for the latter atom, $S_z=-0{\cdot}45$): Cr_{II} (in $\frac{1}{4}\frac{1}{2}\frac{7}{8}$ and $\frac{1}{4}0\frac{3}{8}$) has only z components ($S_z=0{\cdot}86$). The total spins are (Ni)=1·0 and (Cr)=1·11, and the moment values are $\mu(\text{Ni})=2{\cdot}0\ \mu_B$: $\mu(\text{Cr})=2{\cdot}22\mu_B$. The figures are computed from neutron diffraction data given by Prince in 1961. An equivalent model (magnetic twin) has ferrimagnetism along Oy and antiferromagnetic x and z modes. Magnetic interactions are highly anisotropic.

Introduction

$NiCr_2O_4$ is a normal cubic spinel ($Fd3m$–O_h^7 above $T_1=310$°K and becomes tetragonal below T_1 (Delorme, 1955; Lotgering, 1956) with $a_0=5{\cdot}76$, $c_0=8{\cdot}50$ Å. It is generally admitted that the space group of the tetragonal phase is $I4_1/amd$–D_{4h}^{19} (Prince, 1961) with

4Ni in 4(*a*): 000 (1); $0\frac{1}{2}\frac{1}{4}$ (2); $\frac{1}{2}\frac{1}{2}\frac{1}{2}$ (3); $\frac{1}{2}0\frac{3}{4}$ (4)

8Cr in 8(*d*): $0\frac{1}{4}\frac{5}{8}$ (1); $\frac{1}{4}\frac{1}{2}\frac{7}{8}$ (2); $\frac{1}{2}\frac{1}{4}\frac{1}{8}$ (3); $\frac{1}{4}0\frac{3}{8}$ (4)